

Hydrogen adsorption at RuO₂(110)

Qiang Sun, Karsten Reuter and Matthias Scheffler

Fritz-Haber-Institut der Max-Planck-Gesellschaft, Faradayweg 4-6, D-14195 Berlin-Dahlem, Germany

(Dated: November 4, 2018)

The structural, vibrational, energetic and electronic properties of hydrogen at the stoichiometric RuO₂(110) termination are studied using density functional theory. The oxide surface is found to stabilize both molecular and dissociated H₂. The most stable configuration in form of hydroxyl groups (monohydrides) at the undercoordinated O^{br} surface anions is at low temperatures accessed via a molecular state at the undercoordinated Ru^{cus} atoms (dihydrogen) and a second precursor in form of a water-like species (dihydride) at the O^{br} sites. This complex picture of the low-temperature dissociation kinetics of H₂ at RuO₂(110) is in agreement with existing data from high-resolution energy-loss spectroscopy and temperature programmed desorption. Hydrogen adsorption at O^{br} sites increases the reactivity of the neighboring Ru^{cus} sites, which are believed to be the active sites in catalytic oxidation reactions.

PACS numbers: 68.47.Gh, 68.43.Bc, 68.43.Pq, 82.65.+r, 71.15.Mb

I. INTRODUCTION

The widespread use of transition metal (TM) oxides, for example in applications for catalysis, electrochemistry, gas sensors, and corrosion/wear protection is an increasing source of motivation for fundamental research on this material class. An important goal in such studies, focusing on the surface functionality of oxides, is to establish atomic-scale insight into their surface structure and composition, as well as their interaction with gas phase species^{1,2}. Despite notable efforts secure knowledge is still rather scarce. This holds even for well-defined single-crystal surfaces under the controlled conditions of ultra-high vacuum (UHV), mostly due to the structural complexity of oxides and to their often insulating nature which hampers the use of electron spectroscopy techniques³.

With respect to these issues crystalline RuO₂ represents a rather nice choice for a suitable benchmark model system. Not only is it one of the few metallic TM oxides and its rutile bulk structure of modest complexity⁴, but with e.g. a reported high catalytic activity in oxidation reactions^{5,6,7} and being discussed as playing a sensitive role in Pt-Ru based direct methanol fuel cells⁸ it is also sufficiently interesting from an applied perspective. Especially the low energy RuO₂(110) surface has recently received particular attention^{6,7,9,10,11,12,13,14,15,16}. Focusing mostly on the CO oxidation reaction quite some detailed understanding (experimental as well as theoretical) on the fundamental interaction of O and CO with this model surface has emerged from these studies. From the potential interest for both catalytic and fuel cell applications it now appears natural to extend this knowledge also to the interaction of hydrogen with RuO₂(110). From a chemical point of view this ubiquitous gas phase species is expected to form strong bonds particularly with the oxygen anions at the oxide surface². Intentionally or unnoticed hydrogen could therefore be present as surface species in a wide range of conditions, significantly influencing the functionality in the targeted application.

In fact a noticeable effect of hydrogen contamination on the CO turnover numbers has been discussed in a recent experimental study¹⁷.

On a microscopic level Wang *et al.* have provided detailed kinetic and vibrational data on the low-temperature hydrogen adsorption at RuO₂(110) in UHV¹⁸. Using high-resolution electron energy-loss spectroscopy (HREELS) and temperature programmed desorption (TPD) they identified both a molecular and a dissociated hydrogen state, the latter exhibiting vibrational properties of a water-like species with, however, a peculiarly blue-shifted scissor mode. Motivated by these specific results we set out to systematically investigate the structural, vibrational, energetic and electronic properties of hydrogen at the stoichiometric RuO₂(110) surface using density-functional theory (DFT)¹⁹. The stability of molecular and dissociated hydrogen is first discussed at either of the two prominent adsorption sites exhibited by this oxide surface (Section IVA and IVB). Then higher coverages involving simultaneous occupation of both sites are addressed (Section IVC). The detailed picture on the low-temperature dissociation kinetics of H₂ that emerges from the synergetic interplay between computations and experiments is intimately connected with the interesting property of RuO₂(110) to simultaneously sustain both molecular and dissociated hydrogen states, as has already been described briefly in a preceding communication¹⁸.

II. COMPUTATIONAL DETAILS

The DFT calculations were performed within the Full-Potential Linear Augmented Plane Wave (FP-LAPW) method^{20,21,22} using the generalized gradient approximation (GGA)²³ for the exchange-correlation functional. The FP-LAPW basis-set parameters are as follows: R_{MT}^{Ru}=1.8 bohr, R_{MT}^O=1.0 bohr, R_{MT}^H=0.6 bohr, E_{max}^{wf}=20.25 Ry, E_{max}^{pot}=400 Ry, wave function expansion inside the muffin tins up to $l_{max}^{wf}=12$, and potential expansion up to $l_{max}^{pot}=6$. The Brillouin zone integration

employed a $(4 \times 9 \times 1)$ Monkhorst-Pack grid with 18 k-points in the irreducible Brillouin-zone (IBZ) for (1×1) surface unit-cells, and a $(4 \times 4 \times 1)$ grid with 8 k-points in the IBZ for (1×2) cells.

We stress that the very short O-H bonds represent a formidable challenge to electronic structure theory calculations. With respect to the FP-LAPW method employed this translates into the necessity to use rather small non-touching muffin-tin spheres. Then, the convergence behavior with respect to the interstitial plane wave cutoff is rather slow, requiring to use much higher E_{max}^{wf} than the $\sim 17 - 19$ Ry typical for late TM oxide studies involving muffin-tin sphere sizes only dictated by the O-metal bonds. Correspondingly, we tested this convergence by increasing the plane wave cutoff up to 36 Ry (!), as well as by employing denser k-meshes up to 36 k-points in the (1×1) IBZ. From these detailed tests (cf. the appendix), we conclude that the structural and vibrational properties of the systems addressed in the present study are well converged within 0.02 \AA and 8% respectively at the above stated $E_{max}^{wf}=20.25$ Ry, which correspondingly was chosen as our standard cutoff. Relative binding energy differences between configurations involving the same number of O and H atoms (e.g. when comparing tilted and untilted geometries) are similarly well converged to within 0.05 eV at this cutoff. For absolute binding energies on the other hand, in particular when they involve strong O-H bonds like in hydroxyl groups, the chosen, already rather high cutoff is however still not enough. Where such numbers were required within a 0.1 eV/H atom numerical accuracy for our physical argument and are then listed in this manuscript, we correspondingly ran subsequent calculations at a very (say for routine calculations still prohibitively) high cutoff of $E_{max}^{wf}=30$ Ry employing the structure relaxed before at $E_{max}^{wf}=20.25$ Ry. Further, we also checked on the uncertainty introduced by the use of the approximate exchange-correlation functional by performing a number of calculations employing also the local-density approximation (LDA)²⁴ and will comment on the differences between results obtained within LDA and GGA below.

The $\text{RuO}_2(110)$ surface was modelled by a three trilayer O- (Ru_2O_2) -O periodic slab as detailed before^{12,13}, using a vacuum region of about 13 \AA to decouple the interactions between neighboring slabs in the supercell geometry. All structures were fully relaxed by a damped Newton scheme until the residual forces on the atoms were less than 50 meV/\AA , keeping only the atomic positions in the central trilayer at their fixed bulk positions. Test calculations employing 5 and 7 trilayer slabs and relaxing also deeper lying layers showed no significant structural changes beyond the topmost trilayer, neither was there an influence on the atomic surface geometries as obtained with the three trilayer calculations. At this point we would further like to emphasize that the structural relaxation allowed for any symmetry breaking at the surface. This was found to be crucial to obtain the correct energetics and structures, which often involve sig-

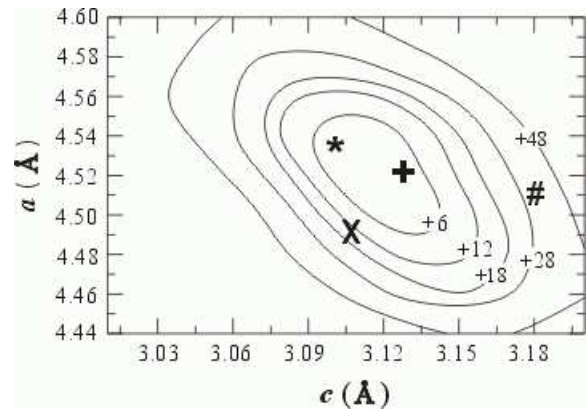


FIG. 1: Computed GGA energy contours as a function of RuO_2 bulk lattice parameters a and c (with optimized internal parameter u). The energy zero corresponds to the optimized values of $a = 4.52 \text{ \AA}$ and $c = 3.13 \text{ \AA}$ marked with '+' and higher contour levels are labelled in the figure in meV per RuO_2 formula unit. Additionally shown are the bulk lattice parameters as determined by experiments ('*' [9], 'x' [27], '#' [28]). The bulk lattice parameters obtained by an earlier DFT-GGA pseudopotential study are $a = 4.65 \text{ \AA}$ and $c = 3.23 \text{ \AA}$ [9], outside of the range shown in the figure.

nificant tilting of the surface groups.

For the calculations of the vibrational modes of the various surface species, the dynamical matrix was set up by displacing each of the involved surface atoms from their equilibrium positions in 0.04 \AA steps. Anticipating a good decoupling of the vibrational modes due to the large mass difference between Ru and O/H, the positions of all atoms in the substrate below the adsorption site were kept fixed in these calculations. The normal modes were then obtained by subsequent diagonalization of the dynamic matrix.

III. BULK RuO_2 , CLEAN (110) SURFACE, FREE H_2 AND H_2O

Summarizing and extending the results of our earlier publications on RuO_2 ^{12,13,14,15,16} we first briefly describe the obtained properties of the bulk and the clean (110) surface, as well as free H_2 and H_2O molecules, as far as they are relevant for the understanding of the hydrogenated surface discussed below.

RuO_2 crystallizes in the rutile structure, described by lattice parameters a and c , as well as one internal degree of freedom u specifying the positions of the O anions within the bulk unit-cell⁴. In order to determine the bulk equilibrium lattice constants we scanned a grid in a and c near the experimental values with 0.02 \AA and 0.015 \AA steps respectively at a high interstitial plane wave cutoff of 30 Ry. At each grid point the internal parameter u was further optimized minimizing the computed forces on the O atoms in the unit-cell. The resulting energy landscape is shown in Fig. 1, while Table I

TABLE I: RuO₂ lattice constants (a , c and u) and bulk modulus (B_0) as determined within LDA and GGA, full-potential (FP) and pseudopotential (PP) calculations. Experimental values are from X-ray diffraction (XRD) and low-energy electron diffraction (LEED) experiments.

	a (Å)	c (Å)	u	B_0 (GPa)
This work (FP-LDA)	4.42	3.05	0.306	352
This work (FP-GGA)	4.52	3.13	0.306	294
[25] (PP-LDA)	4.56	3.16	0.307	283
[9] (PP-GGA)	4.65	3.23	0.305	–
[26] (XRD)	4.492	3.106	0.306	270
[27] (XRD)	4.491	3.106	–	–
[28] (LEED)	4.51	3.18	–	–
[9] (LEED)	4.51	3.23	–	–

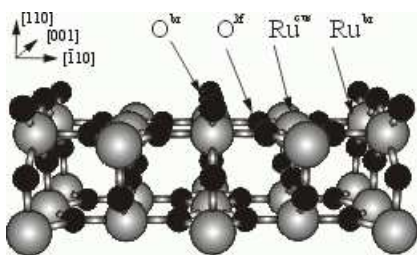


FIG. 2: Side view of the stoichiometric RuO₂(110) surface termination explaining the location of the two prominent adsorption sites corresponding to under-coordinated surface atoms: bridging oxygen O^{br} and coordinatively unsaturated (cus) ruthenium Ru^{cus} (Ru = light, large spheres; O = dark, small spheres).

lists the determined bulk lattice parameters within the LDA and GGA. Comparing with available bulk diffraction studies^{26,27} we obtain very good agreement within the GGA. Interestingly, two earlier DFT pseudopotential calculations (LDA²⁵ and GGA⁹) yield larger lattice parameters that deviate by more than 0.1 Å from our LDA and GGA values, respectively. We particularly checked on the GGA value by Kim *et al.*, but find their geometry to be about 0.4 eV per RuO₂ formula unit higher in energy than our ground state geometry. Tentatively, we take this 0.1 Å and 0.4 eV as a rough estimate of the structural and energetic error introduced by the pseudopotential approximation when describing late transition metal (TM) oxide compounds. Finally, we notice that the c lattice parameter measured in two independent low-energy electron diffraction (LEED) experiments^{9,28} deviates from the bulk diffraction results by about 0.1 Å. In both LEED experiments thin RuO₂(110) films grown on Ru(0001) were investigated, where the c lattice parameter corresponds to the size of the surface-unit cell in the [001] direction. Apparently, a thin film (with an incommensurable structure to that of the metal substrate) prefers a slightly different geometry than a bulk crystal.

Depending on the oxygen-content in the surrounding gas phase, either a stoichiometric or an oxygen-rich termination is stabilized at the RuO₂(110) surface^{12,16}. Figure 2 shows the surface geometry of the stoichiometric termination exhibiting two kinds of surface species, the nearest neighbor shell of which has been reduced by the creation of the surface: A twofold coordinated bridging oxygen O^{br} (threefold coordinated in the bulk) and a fivefold coordinated ruthenium atom Ru^{cus} (sixfold coordinated in the bulk). The only other surface species present, O^{3f}, still maintains its bulk-like threefold coordination to in-plane Ru atoms. The oxygen-rich termination differs from this geometry only by extra oxygen atoms adsorbed on-top of the Ru^{cus} atoms. In the following we will focus exclusively on the interaction of hydrogen with the stoichiometric termination, attempting to make contact with the existing data from ultra-high vacuum (UHV) experiments¹⁸, where the stoichiometric termination is the standard surface produced after a high-temperature anneal to 600 K^{6,9,10,11}. The discussion of hydrogen interaction with the oxygen-rich termination is deferred to a consecutive publication.

Due to the cutting of bonds the surface atoms relax. Most prominently we find that the O^{br} atoms move inwards, reducing their bond length to the underlying Ru atoms (henceforth denoted Ru^{br}) to 1.91 Å (bulk: 1.99 Å), and, correspondingly, the inter-layer distance is reduced to 1.09 Å (12% smaller than bulk). These findings are in very good agreement with a recent LEED study which determined a bond length of 1.94 Å and a first layer contraction of -13% at RuO₂(110)⁹, and they are similar to the geometric changes observed at the isostructural TiO₂(110) surface²⁹. Although not as pronounced also the under-coordinated Ru^{cus} atoms relax a bit inwards, thereby inducing a buckling within the first trilayer plane of 0.16 Å (LEED: 0.18 Å). Contrary to other transition metal oxide surfaces like e.g. Al₂O₃(0001)³⁰ the structural relaxations are therefore rather small, and in particular damp away rapidly: No significant deviations from the bulk-like positions are found for atoms below the first trilayer, neither in LEED, nor in our thicker slab test calculations.

Finally, we summarize in Table II the computed binding energies, bond lengths and frequencies for gas phase H₂ and H₂O. For both molecular and atomic calculations we employed the same muffin-tin spheres as detailed before for the slab calculations, and allowed for non-spherical densities by reducing the symmetry. The total energies for the isolated, spin-polarized atoms are obtained by adding to the total energy value from a non-spin-polarized FP-LAPW calculation a constant spin-polarization energy of 1.52 eV (O) and 1.10 eV (H) taken from a relativistic atomic DFT calculation²⁰. With respect to structural and vibrational properties we obtain very good agreement with the experimental data, as well as with previous DFT studies^{34,35,36}. The slow convergence of the O-H bond energetics already described in the preceding section exists similarly for the free molecules,

TABLE II: Structure parameters (bond length d and angle), binding energy E_b , and vibrational frequencies ν for gas phase H_2 and H_2O . Compared are the computed values for LDA and GGA (at two different LAPW cutoffs) with the corresponding experimental data (with zero-point energy removed).

	LDA		GGA		Exp.
	20.25 Ry	30 Ry	20.25 Ry	30 Ry	
H_2					
d_{H-H} (Å)	0.77	0.77	0.75	0.75	0.74 [31]
E_b (eV)	4.79	4.87	4.45	4.56	4.73 [31]
$\nu_{stretch}$ (meV)	—	—	538	—	546 [32]
H_2O					
d_{O-H} (Å)	0.98	0.98	0.97	0.97	0.96 [32]
\angle_{HOH} (deg)	102	102	103	103	104.5 [32]
E_b (eV)	11.08	11.49	10.04	10.40	10.06 [33]
ν_{sym} (meV)	—	—	424	—	454 [32]
ν_{asym} (meV)	—	—	435	—	466 [32]
$\nu_{scissor}$ (meV)	—	—	189	—	198 [32]

which is why we list the computed values both at the routine 20.25 Ry and at the very high LAPW cutoff of 30 Ry (used later on to obtain quantitative binding energies as discussed above). With respect to the latter cutoff we assess the numerical convergence of the gas phase binding energies to be within 0.2 eV. This points then at a sizable error (i.e. overbinding) compared to the experimental values when oxygen is involved even within the GGA, which is a well known result²³. Although some error cancellation occurs in the computation of binding energies at surfaces (as illustrated in the appendix), we conclude that a cautious reasoning is necessary when judging on the endo- or exothermicity of adsorption with respect to the gas phase molecules. To this extent most of our physical arguments will instead rather be based on binding energy *differences*, which are more accurately described (± 0.05 eV, cf. the appendix).

IV. THE HYDROGENATED $RuO_2(110)$ SURFACE

In the following sections we systematically discuss the hydrogen interaction with the various surface species present at the stoichiometric $RuO_2(110)$ termination. The energetics will be described with respect to the afore-described free H_2 molecule, where a negative binding energy denotes endothermicity with respect to the gas phase species and the bare surface, i.e. a metastable situation. As we find the interaction with the threefold coordinated in-plane O^{3f} to be energetically very unfavorable (even the formation of a monohydride is endothermal by ≈ -0.3 eV/H atom), the discussion will concentrate on the two under-coordinated surface species, i.e., Ru^{cus} and

O^{br} . At first we discuss hydrogen first to be present at one of these sites only (Section IVA and IVB). And then we consider simultaneous adsorption at both sites (Section IVC). Consistent with our previous publications we will employ a short hand notation to characterize the manifold of studied geometries, indicating first the occupancy of the bridge site and then of the cus site, e.g. $(OH)^{br}/H_2^{cus}$ for a configuration with an OH-group at the bridge site and a H_2 molecule at the cus site.

Lateral interactions between functional groups at directly neighboring cus and bridge sites are implicitly contained within our calculations employing (1×1) surface unit-cells. With these cells only integer multiples of one monolayer (ML) hydrogen coverage can be studied (1 ML defined as monoatomic occupation of all sites of one type (br or cus)). Further reaching lateral interactions, e.g. towards a moiety at the same site type either along $[\bar{1}10]$ (at a distance of 6.4 Å) or along $[001]$ (at a distance of 3.1 Å, see Fig. 3) could lead to the formation of more dilute superstructures with fractional MLs hydrogen coverage. From a systematic study of oxygen adsorption at $RuO_2(110)$ we find such lateral interactions to be rather small at this rather open oxide surface³⁷ and don't expect this to be significantly different for hydrogen, in particular along the longer $[\bar{1}10]$ direction of the surface unit-cell, where the next-nearest site would be 6.4 Å away. Correspondingly, we only test for lateral interactions in selected configurations employing larger (1×2) cells, allowing us to model structures where then only every second site is occupied along the $[001]$ direction (see e.g. Fig. 7 below).

A. Hydrogen at Ru^{cus}

We start with the molecular adsorption of H_2 at the under-coordinated Ru^{cus} site (O^{br}/H_2^{cus}). This analysis was motivated by the aforementioned recent UHV HREELS experiments that attributed a weak peak at 367 meV to the stretch mode of a molecular hydrogen species at the surface with a TPD activation energy of about 0.3 eV¹⁸. Relaxing a H_2 molecule in (1×1) cells from a height at about 2 Å atop the cus sites our calculations indeed find such a (meta)stable species with a computed binding energy of +0.32 eV/ H_2 with respect to molecular H_2 . The resulting adsorption geometry is shown in Fig. 3 together with the calculated vibrational modes. At a height of 1.85 Å the H_2 molecule lies parallel to the surface above the cus sites (side-on configuration). Interestingly, we find almost no corrugation of the potential energy surface with respect to an azimuthal rotation of the flat-lying H_2 molecule: The optimal bond orientation about 30° degree from the $[\bar{1}10]$ direction is only by insignificant 3 meV more stable than any other orientation, i.e. the H_2 behaves essentially like a free-rotator (helicopter mode), as also reflected by the very low rotational vibration frequency of 12 meV, cf. Fig. 3. The similarly low in-plane translational modes further point

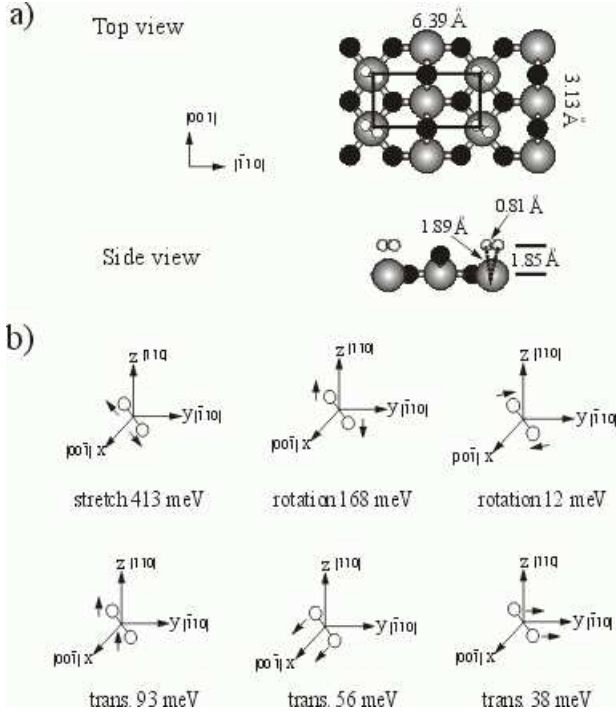


FIG. 3: a) Top and side view of the adsorption geometry of 1 ML H_2 at Ru^{cus} (Ru = light, large spheres; O = dark, small spheres; H = white, small spheres). Additionally shown is the size of the (1×1) surface unit-cell. Note that the azimuthal direction of the plotted H_2 is arbitrary, as it is freely rotating. b) Six vibrational modes of the adsorbed H_2 molecule. The directions and lengths of the arrows indicate approximately the directions and relative magnitudes of the displacements of the atoms.

at a rather expressed delocalization of the H_2 molecule parallel to the surface, particularly in the $[\bar{1}10]$ direction, i.e. approaching the neighboring bridging oxygens. Despite this the H_2 bond length is with 0.81 \AA noticeably stretched compared to the free gas phase molecule (0.75 \AA). This is consistent with the rather high binding energy and the significantly decreased stretch vibration (413 meV compared to 538 meV in the gas phase).

These properties reflecting a moderately strong interaction are very similar to molecular H_2 at late transition metal surfaces (like e.g. $\text{Pd}(100)^{38}$) if adsorption is restricted to take place at the on-top site. Of course, at the latter surfaces the on-top site is only a local “constrained” minimum and H_2 would dissociate towards higher-coordinated hollow sites. The different geometry of $\text{RuO}_2(110)$ doesn’t offer such sites, thus stabilizing the molecular adsorption at Ru^{cus} . In this respect we attribute the non-dissociative interaction of H_2 with these sites more to a geometry effect, rather than to an electronic effect, i.e. compared with the weak physisorption of H_2 at noble metal surfaces like $\text{Ag}(111)^{39}$.

The relatively strong interaction (electron polarization and bond formation) is also obvious in the “difference density” plot shown in Fig. 4. The “difference density” is

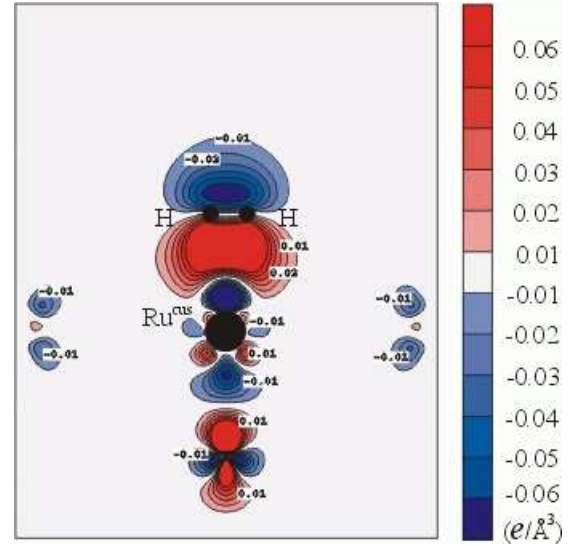


FIG. 4: Difference density plot for H_2 adsorbed at Ru^{cus} . The contour plot depicts the plane parallel to the H_2 molecular axis and normal to the surface. Areas of electron accumulation and depletion have positive and negative signs respectively, contour lines are drawn at 0.01 e/\AA^3 intervals.

obtained by subtracting from the electron density of the adsorbate system that of the clean surface and that of the free molecule (the latter two with the same interatomic distances as found for the adsorbate system)⁴⁰. A rather strong polarization of the flat-lying H_2 is apparent, with electron density accumulation on the substrate side of the molecule and depletion on the vacuum side. Due to the interaction with the H_2 the back-bond of the Ru^{cus} atom to the underlying O substrate atom is slightly weakened, the Ru atom moves 0.03 \AA upwards and thereby reduces the clean-surface-buckling in the topmost trilayer.

The structure of the difference density plot suggests the major interaction in the occupied states to be due to a hybridization of $\text{Ru}-d_{z^2}$ and $\text{H}_2-\sigma$ orbitals. Analyzing the computed local density of states we indeed find the bonding governed by this and a smaller hybridization of the $\text{Ru}-d_{xz}/d_{yz}$ with the $\text{H}_2-\sigma^*$ orbitals. The bonding of the H_2 molecule to the cus site can therefore be understood within the familiar donation/back-donation picture⁴⁰, where the hybridization with the $\text{H}_2-\sigma$ orbital causes a small $\text{H}_2 \rightarrow \text{Ru}$ charge transfer that is counteracted by some back-donation of electronic charge from the metal to the $\text{H}_2-\sigma^*$ level, strengthening the coupling to the substrate while weakening and elongating the H-H bond.

Contrary to the situation at most more reactive TM surfaces this back-donation is however not strong enough to completely dissociate the H_2 molecule. This is supplemented by the surprising result that atomic hydrogen is not stable at the Ru^{cus} site: We compute only an endothermal binding energy of -0.33 eV/H atom with respect to $1/2 \text{ H}_2$ at 1 ML H-coverage, i.e. in (1×1) unit-cells. Checking whether H bonding might become

more favorable in more dilute superstructures we also employed (1×2) cells to model a 0.5 ML H-coverage with H only at every second site along the $[001]$ direction. With -0.20 eV/H atom with respect to $1/2$ H_2 the binding energy is still endothermal and only slightly changed, reflecting the small lateral interactions at the $RuO_2(110)$ surface. Expecting no further changes in binding energy for even more dilute H-phases we therefore conclude that only molecular hydrogen may be stabilized at the cus sites.

Forming the basis for e.g. relations between heterogeneous and homogeneous catalysis it is interesting to compare these findings for the Ru atom at the surface of an oxide with the hydrogen bonding to TM atoms in other frameworks like e.g. at the surface of metals or in a TM complex. As already mentioned, coupling of hydrogen to TM surfaces is generally associated with the dissociation of the ligand⁴¹. The observation of non-dissociative chemisorption of H_2 has so far been restricted to a few exceptional cases^{42,43}, mostly connected with a prior saturation of the most reactive sites at the surface with atomic hydrogen. Concomitantly, we compute e.g. the bonding of atomic H at $Ru(0001)$ to be exothermic at least up to 1 ML coverage. Molecular precursors have more been identified at noble surfaces like $Ag(111)$ ³⁹, yet then physisorbed and certainly not exhibiting such a strong activation of the H_2 bond as expressed at $RuO_2(110)$ with the significant bond elongation and downshift of the stretch frequency. These findings resemble much more the data from organometallic complexes: For so-called η^2-H_2 (dihydrogen) single metal atom complexes, in which the H-H bond remains intact⁴⁴, TM- H_2 bond energies in the range of 0.1-0.3 eV/ H_2 are estimated⁴⁵, significant red-shifts of the stretch frequency^{45,46} and bond elongation up to 0.9 Å are reported^{47,48}. In fact, neutron scattering experiments furthermore indicate rapid rotation of η^2-H_2 ligands with an activation energy of less than about 10 meV⁴⁷, just as we find for the molecular hydrogen at Ru^{cus} . Even the donation/back-donation bonding model is analogously discussed for the TM complexes⁴⁹. Yet, there (just like at TM surfaces) the back-donation may also break the H-H bond, and often H_2^- as well as H-ligands are attached to the same metal center and can even exhibit continuous changes between both configurations^{45,46}. At $RuO_2(110)$, in contrast, the bonding to the surrounding oxide apparently depletes the electron density at the under-coordinated Ru^{cus} atom already in such a way, that the back-bonding only activates the H_2 bond, but may no longer break it.

B. Hydrogen at O^{br}

For H_2 molecules approaching the RuO_2 surface at the under-coordinated O^{br} atoms we find that they will either slide towards the Ru^{cus} sites or that they are repelled into the gas phase. In no case (i.e., testing many H_2 ori-

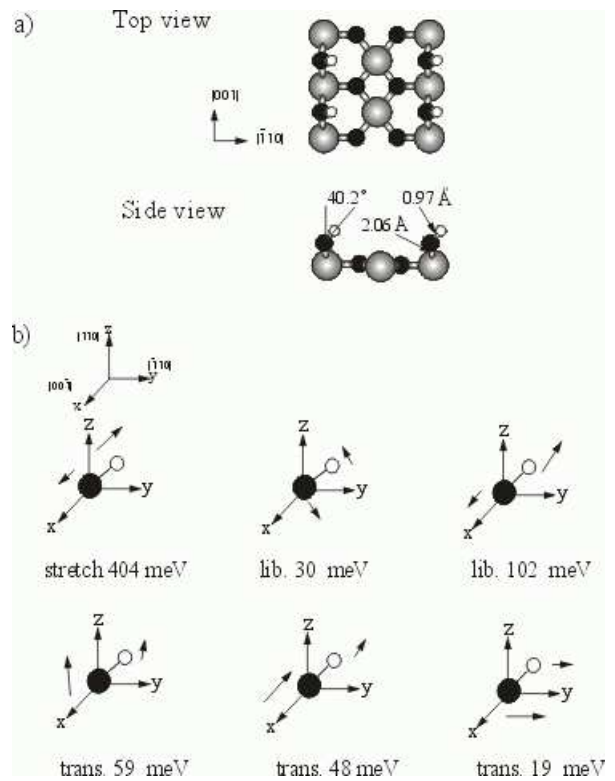


FIG. 5: a) Top and side view of the adsorption geometry of 1 ML H at O^{br} , computed in (1×1) unit-cells. b) Six vibrational modes of the formed hydroxyl group.

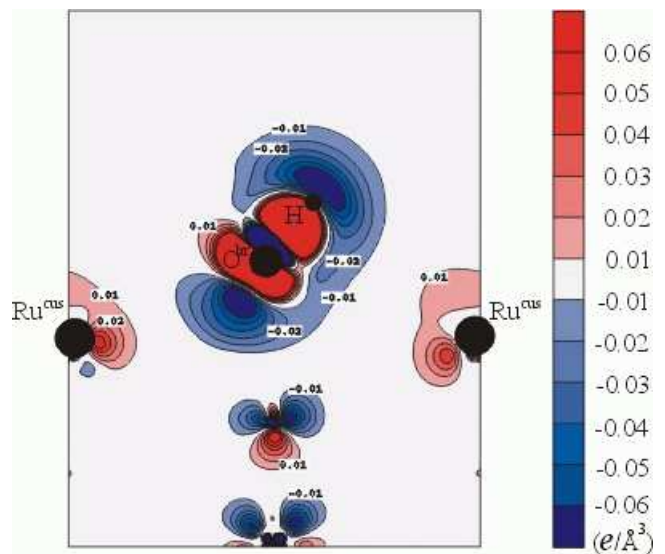


FIG. 6: Difference density plot of a hydroxyl group at the bridge sites $(OH)^{br}/-$. The contour plot depicts the plane parallel to $[110]$ and normal to the surface. Areas of electron accumulation and depletion have positive and negative signs respectively, contour lines are drawn at 0.01 $e/\text{\AA}^3$ intervals.

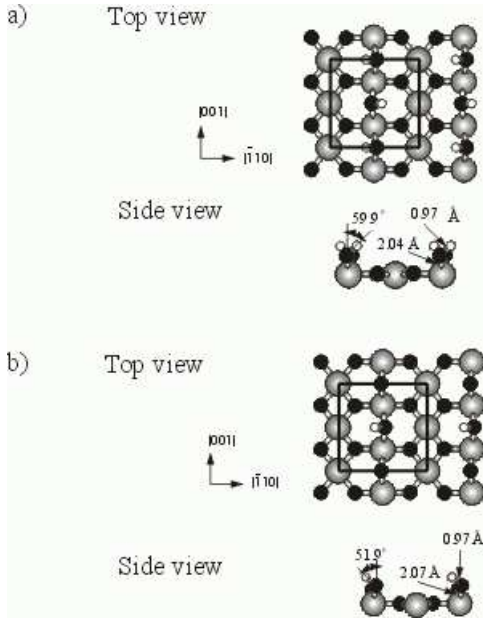


FIG. 7: a) Top and side view of the adsorption geometry of 1 ML H at O^{br} , computed in (1×2) unit-cells with alternating tilting. b) Top and side view of the adsorption geometry of 0.5 ML H at O^{br} .

entations, as well as lower coverages in a (1×2) cell) did we observe spontaneous dissociation above the O^{br} site. This leads us to conclude that molecular adsorption primarily takes place over the aforesaid cus sites. Atomic hydrogen, on the other hand, binds at the O^{br} sites, i.e., forming a surface hydroxyl group. The optimized geometry of the 1 ML $(OH)^{br}/-$ phase computed in (1×1) cells is shown in Fig. 5. The strong binding within the OH-group weakens the bond to the underlying Ru^{br} substrate atoms and elongates it significantly from 1.91 Å to 2.06 Å. The surface OH-group itself has a bond length of 0.97 Å, nearly identical to the O-H distance in H_2O , and is inclined towards the $[\bar{1}10]$ direction with a 40° angle with respect to the surface normal. The computed binding energy is +0.89 eV/H atom stronger than in molecular H_2 , and the energy gain by the tilting is 0.1 eV/H atom compared to the higher-symmetry, upright configuration. Again, both the computed stretch frequency, as well as the binding energy are found to be in good agreement with the recent HREELS and TPD data from the hydroxylated surface¹⁸, and the strong binding is also nicely visible in the difference density plot shown in Fig. 6.

With only a 0.1 eV energy difference between tilted and upright position, the hydroxyl groups will at finite temperatures frequently swing from one orientation to the other. Checking whether this may occur in concerted wave-like motions along a chain of bridge sites, we repeated the calculation with 1 ML coverage, but now in a (1×2) cell with each OH-group alternatingly tilted in one or the other direction as shown in Fig. 7a. The only structural difference obtained is a somewhat larger

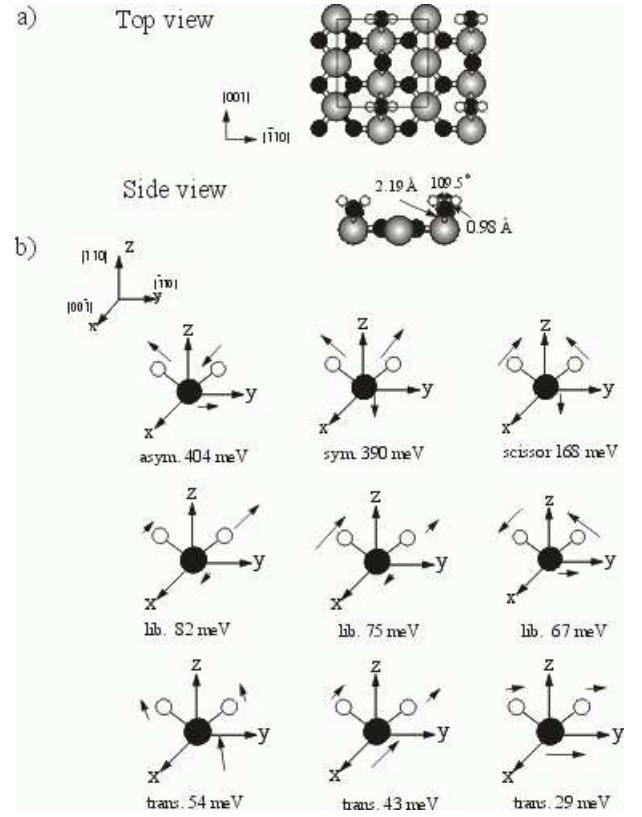


FIG. 8: a) Top and side view of the adsorption geometry of 0.5 ML water-like species at the bridge sites, oriented along the $[\bar{1}10]$ direction. b) Corresponding nine vibrational modes.

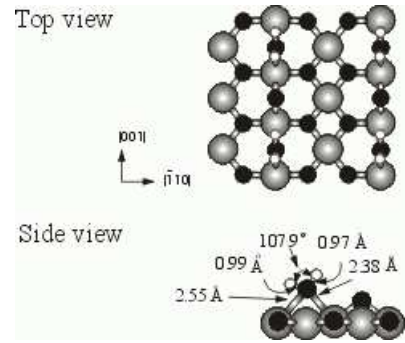


FIG. 9: Top and side view of the adsorption geometry of 0.5 ML water-like species at the bridge sites, oriented along the $[001]$ direction.

tilt angle of about 60° degree, while bond length and binding energy remain to within 0.01 eV/H atom virtually unchanged. Testing for further reaching lateral interactions by decreasing the total coverage to 0.5 ML as shown in Fig. 7b, we again find the binding energy within 0.02 eV/H atom degenerate to the previous two cases, leading us to conclude that each OH-group tilts and swings essentially independent of the others, and of the total coverage which may thus easily reach the full 1 ML with each O^{br} atom hydroxylated.

The low temperature HREELS and TPD experiments by Wang *et al.*¹⁸ show that the coverage of dissociated hydrogen can be increased above 1ML. There is evidence for a hydrogen state at O^{br} , that exhibits frequencies resembling a water-like H-O-H configuration, i.e. with two H atoms per bridge site (dihydride). Surprisingly, the measured scissor mode for this functional group is with 231 meV higher than the one of gas phase water (exp: 198 meV, calc: 189 meV, see Table II), whereas intuitively a red-shift would be expected: Considering that the molecule-surface interaction weakens the intra-molecular bonds and normally widens the H-O-H angle, both these effects would rather tend to make the bending mode softer⁴¹. Trying to address this puzzling finding we computed such water-like configurations at the bridge sites first at 1 ML H_2O -coverage in (1×1) cells and with the water-axis oriented once along $[001]$ and once along $[\bar{1}10]$. Both configurations exhibit only a very low stability and can thus not account for the experimental water-like species with a desorption temperature around 300 K¹⁸. We therefore proceeded to relax the same two configurations at lower coverages in (1×2) cells with water-like species now only at every second bridge site as shown in Figs. 8 and 9. While the model with orientation along the $[001]$ axis is still slightly endothermal, the binding energy of the other orientation shown in Fig. 8 finally turns out already at least exothermal by $+0.48 \text{ eV}/H_2$. Still, as almost expected the calculated scissor mode for this configuration (just as much as the one of the other three models) is with 168 meV significantly lower than the one of free water, and thus in strong disagreement with the experimental data.

Recalling the strong tilting of the mono-hydride group at O^{br} shown in Fig. 5 we then tested to similarly tilt the whole water-like species of the last most favorable model and ended up with the geometry shown in Fig. 10, that is apparently separated from the up-right configuration by a sizable energy barrier (i.e. neither configuration relaxes automatically into the other one). The tilt not only significantly increases the binding energy of this configuration by 0.08 eV to $+0.56 \text{ eV}/H_2$, but also the computed scissor mode is with 211 meV 12% higher than the one of a free water molecule (189 meV, see Table II). Also the other computed vibrational modes listed in Fig. 10b are now in reassuring agreement with the experimental HREELS data (exp: stretch 436 meV, scissor 231 meV, libration 110 meV 76 meV, translation 59 meV 28 meV)¹⁸.

The question remains why this tilted geometry gives rise to the counterintuitively blue-shifted scissor mode. Inspecting the relaxed geometry displayed in Fig. 10 in more detail we find the water-like H-O-H bond angle with 108° slightly increased compared to free water (calculation: 103° , see Table II), lending more towards the argument favoring a weakening of the bending mode. However, this angle together with the overall tilting of the whole functional group causes the lower OH-bond of the water-like species to end up almost parallel to the surface (only 8° to the surface plane), bringing the

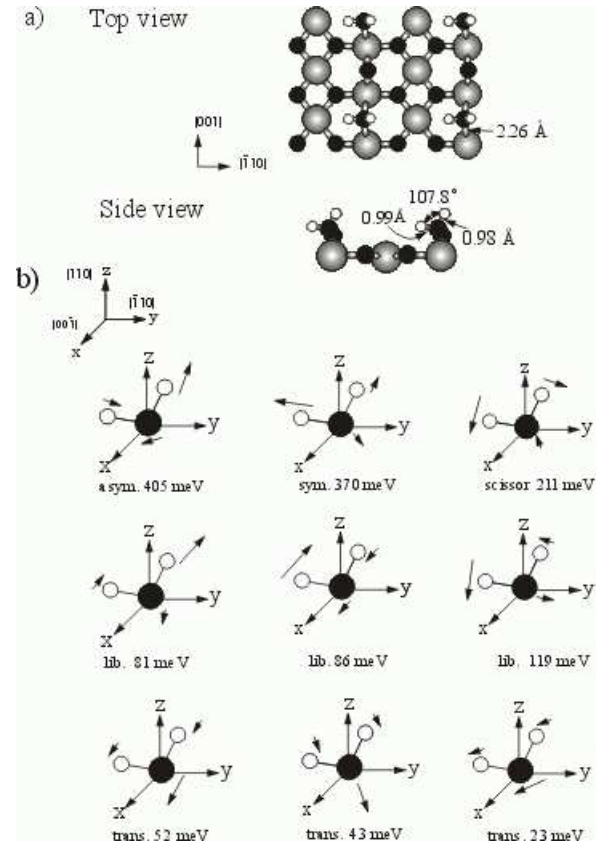


FIG. 10: a) Top and side view of the adsorption geometry of 0.5 ML water-like species at the bridge sites, oriented asymmetrically along the $[\bar{1}10]$ direction. b) Corresponding nine vibrational modes.

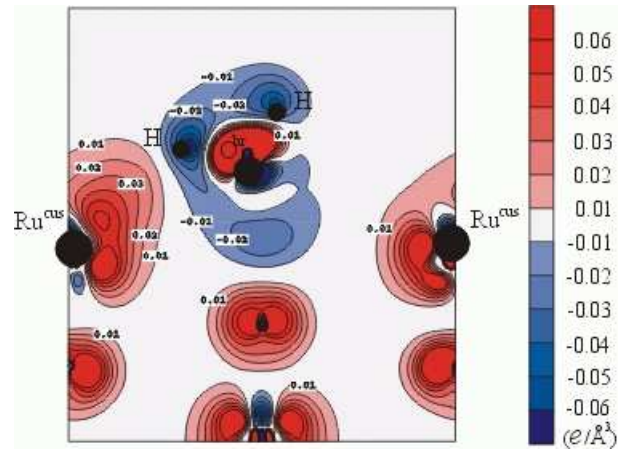


FIG. 11: Difference density plot of the asymmetric water-like species of Fig. 10 at the bridge sites. The contour plot depicts the plane parallel to $[\bar{1}10]$ and normal to the surface. Areas of electron accumulation and depletion have positive and negative signs respectively, contour lines are drawn at $0.01 \text{ e}/\text{\AA}^3$ intervals.

terminal H atom closer to the neighboring Ru^{cus} atom (2.72 Å compared to 3.19 Å in the upright model shown in Fig. 8). This suggests a possible interaction between these two species that is indeed verified by inspecting the computed difference density plot shown in Fig. 11. Although small, the apparent hydrogen bridge bonding possible in this tilted configuration hinders any movement away from Ru^{cus} parallel to the $[\bar{1}10]$ direction and thus naturally stiffens not only the scissor mode, but also the corresponding librational mode (calc: 119 meV, exp: 110 meV, compared to “typical” values around 80 meV, cf. Figs. 10 and 8).

This intricate coupling between neighboring bridge and cus sites fits nicely into the picture of the low temperature dissociation kinetics of H_2 at $\text{RuO}_2(110)$ that emerges from the data presented in Sections IVA and IVB, as well as from the detailed UHV-HREELS experiments by Wang *et al.*¹⁸. Although the thermodynamic ground state for hydrogen at this stoichiometric surface is given by the strongly bound hydroxyl-groups at the bridge sites (binding energy +0.89 eV/H atom)¹⁶, direct dissociation over these sites is apparently inhibited at least at low temperatures by an energy barrier. Thus, we tend to conclude on the following scenario: When H_2 interacts with $\text{RuO}_2(110)$, it is at first bound in molecular form at the cus sites (binding energy +0.16 eV/H atom). Although the H_2 bond is weakened in this process, the cus sites can not induce its complete cleavage. This is instead achieved via the water-like metastable configuration at the bridge sites (binding energy +0.28 eV/H atom) that may be accessed from the molecular H_2 state at the cus sites (as indicated by the low translational mode in $[\bar{1}10]$ direction, cf. Fig. 3). From there the hydroxyl groups are finally formed, presumably by activated hydrogen diffusion. This interpretation of H_2^{cus} as a necessary precursor state to dissociation is also supported by new low temperature HREELS and TDS experiments which report a suppressed population of the water-like species at bridge if the cus sites are first blocked by CO molecules⁵⁰. Only if the water-like species are allowed to form, the hydroxyl groups result from moderate heating to 350 K¹⁸.

C. Hydrogen at both sites: Higher coverages

Having discussed the lower coverage adsorption up to 1 H_2 -ML for both sites separately, we now proceed to higher total coverages involving hydrogen at both sites. Also with various hydrogen functional groups present at the bridge sites we still find atomic hydrogen at cus to be always unstable. Correspondingly we restrict our detailed discussion to molecular H_2 at cus and different hydrogen populations at the bridge sites. Starting with the water-like species at bridge, the (1×1) configuration $(\text{H}_2\text{O})^{\text{br}}/\text{H}_2^{\text{cus}}$ corresponding to a total coverage of 2 H_2 -ML is computed to be endothermic, reflecting presumably already an oversaturation of the surface with hydrogen. This improves in more dilute (1×2) con-

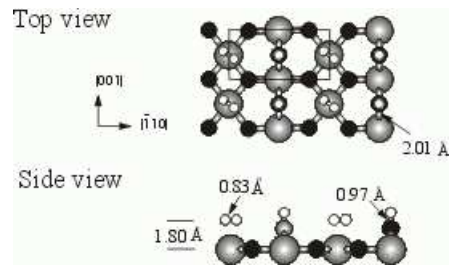


FIG. 12: Top and side view of the adsorption geometry of the 3 H_2 -ML $(\text{OH})^{\text{br}}/\text{H}_2^{\text{cus}}$ phase.

figurations with $(\text{H}_2\text{O})^{\text{br}}$ and H_2^{cus} occupying only every other site. The average binding energy for both a checkerboard arrangement and with both species occupying directly neighboring sites turns then out exothermic by about +0.2 eV/ H_2 , with a slight preference for the checkerboard arrangement in which the two hydrogen species maximize their mutual distance. This average binding energy is, however, still lower than the average binding energy we obtained for the (1×1) $\text{O}^{\text{br}}/\text{H}_2^{\text{cus}}$ phase (+0.32 eV/ H_2 , cf. Section IVa) which also corresponds to a total coverage of 1 H_2 -ML.

This leaves as interesting higher coverage phase beyond 1 H_2 -ML only the possibility to combine H_2^{cus} with hydroxyl groups at the bridge sites. For this remaining combination even a dense (1×1) arrangement of $(\text{OH})^{\text{br}}/\text{H}_2^{\text{cus}}$ at 1.5 H_2 -ML total coverage turns out very stable with an average binding energy of +0.6 eV/ H_2 . This points at the possibility that after the aforesaid formation of hydroxyl groups at bridge also the molecular state at the cus sites could simultaneously be populated upon continued hydrogen uptake. In other words that the $\text{RuO}_2(110)$ surface offers the fascinating property that hydrogen may coexist both in the dissociated monohydride and in the non-dissociated dihydrogen state. Inspecting the corresponding geometry shown in Fig. 12, the first striking effect of the simultaneous occupation of bridge and cus states is that the pronounced tilting of the hydroxyl group, cf. Fig. 5, has disappeared. Next, the H_2 at the cus sites is apparently more activated compared to the situation discussed in Section IVA when the bridging oxygen atoms were bare: The bond length is increased from 0.81 Å to 0.83 Å, and the molecule resides at 1.80 Å height, i.e. 0.05 Å closer to the surface.

Interestingly, the formation of the hydroxyl group at the bridge sites seems to influence the bonding properties at the neighboring cus sites, rendering the latter somewhat more reactive. The mechanism with which this happens is nicely identified on the basis of the difference density plot shown in Fig. 13. Plotted are the induced electron density variations arising in the $(\text{OH})^{\text{br}}/\text{H}_2^{\text{cus}}$ phase when the hydroxyl group is formed. Apart from the obvious significant density rearrangement at the bridge sites themselves (which is very similar to the one shown in Fig. 6 for the lower coverage $(\text{OH})^{\text{br}}/-$ phase), also some variations can be observed at the distant cus sites:

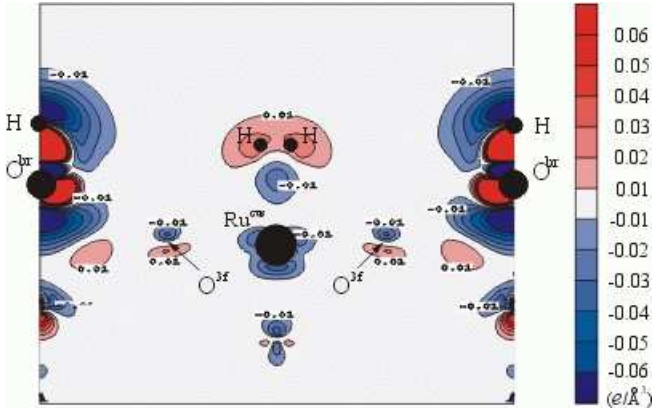


FIG. 13: Difference density plot of the high coverage (1×1) $(\text{OH})^{\text{br}}/\text{H}_2^{\text{cus}}$ phase shown in Fig. 12. Displayed are the induced electron density changes in the system when hydrogen forms a hydroxyl group at the bridge sites. The contour plot depicts the plane normal to the surface that cuts through a bridge site and its next-nearest neighbor cus site (this way passing very close a $\text{O}^{3\text{f}}$ atom and the positions which are nearest to the $\text{O}^{3\text{f}}$ are indicated by arrows). Areas of electron accumulation and depletion have positive and negative signs, respectively, contour lines are drawn at $0.01 \text{ e}/\text{\AA}^3$ intervals.

electron density is depleted around the Ru^{cus} atoms and clearly populates the H_2 σ^* -orbital, thereby weakening the molecular bond. At the same time the H_2 -metal bond is strengthened, so that the absolute binding energy is only slightly altered ($0.23 \text{ eV}/\text{H}_2$ compared to the $0.32 \text{ eV}/\text{H}_2$ without the presence of the hydroxyl group, cf. Section IVA). Still, the molecule is more activated and adsorbs closer to the surface.

We interpret the surface's capability to give a higher back-donation to the cus bond upon population of hydroxyl groups at bridge as arising from an interesting bond order propagation effect. Due to the newly formed hydroxyl bond the O^{br} atoms become less bound to the underlying Ru^{br} atoms, as reflected by the considerable increase in bond length from 1.91 \AA to 2.01 \AA . Having thus lost a bit of their optimum bonding environment, the Ru^{br} seek to fortify their remaining back-bonds, among others also to the directly coordinated in-plane $\text{O}^{3\text{f}}$ atoms, cf. Fig. 2. The resulting electron density rearrangement at the latter atoms can nicely be discerned in Fig. 13, which displays a plane connecting next-nearest neighboring bridge and cus sites and thus passes also closely by the $\text{O}^{3\text{f}}$ sites. With this slightly strengthened bond to the Ru^{br} atoms the $\text{O}^{3\text{f}}$ atoms in turn adapt by weakening their bonds to the Ru^{cus} atoms. Due to this propagation of bond order the latter atoms find themselves in a neighborhood that is less electron demanding, allowing for an increased back-donation into the H_2 - Ru^{cus} bond.

While we find further reaching lateral interactions at this surface (e.g. the aforesaid low coupling between hydroxyl groups at neighboring cus sites) to be rather small, the bonding properties at nearest-neighboring

bridge and cus sites are thus obviously under a non-negligible mutual influence. This suggests that one could attempt to tune the reactivity of either site by a controlled population of the respective other site. Particularly for oxidation reactions at $\text{RuO}_2(110)$ several studies have already emphasized the key role played by the cus sites^{6,9,10,11,13,15}. Correspondingly, modifications at the bridge sites like the present decoration with hydroxyl groups could have a noticeable impact on the overall catalytic activity of the surface – not only because of a possible site-blocking of bridge sites, but also because of an intricate tuning of the electronic structure at the cus sites. So far, all reaction mechanisms discussed at this $\text{RuO}_2(110)$ surface have been found to be initial-state dominated, i.e. the reaction barriers scaled with the binding energies of the adsorbed reactants^{7,13}. The above described increased electron-donation ability of the cus sites upon hydroxylation of the bridge sites might therefore likely lead to a different reactivity of this oxide surface. Concomitantly we notice that a promoting effect of small amounts of hydrogen on the CO oxidation reaction over polycrystalline RuO_2 has already been reported in a recent experimental study, proposing this material as a suitable candidate for the technologically important low-temperature CO oxidation in humid air¹⁷. The present work identifies an increased reactivity of the cus sites after hydroxylation of the bridge sites at $\text{RuO}_2(110)$. Further work involving atom-specific Surface Science experiments on the reactivity of hydrogenated RuO_2 surfaces is now required to check if this can be exploited not only for total oxidation reactions, but possibly even more important for partial oxidation, where a controlled tuning of the reactive sites might be crucial to obtain a high selectivity.

V. SUMMARY

In conclusion we presented a detailed *ab initio* study of the energetic, electronic, structural and vibrational properties of hydrogen at the stoichiometric $\text{RuO}_2(110)$ termination. A different interaction with the two undercoordinated, prominent adsorption sites at this surface is found: At Ru^{cus} only a molecular state can be stabilized, while the thermodynamic ground state is represented by hydroxyl groups involving the O^{br} surface atoms. The results strongly suggest that the low-temperature H_2 dissociation takes place via a precursor where molecular H_2 is bound at the Ru^{cus} site. From there a water-like dihydride state at O^{br} can be accessed that leads to the final hydroxyl groups. This emerging picture of the low-temperature dissociation kinetics has been developed in a synergetic interplay with the experimental group of Jacobi and Ertl, and is in full agreement with their HREELS and TDS data¹⁸, in particular with the peculiar blue-shifted scissor mode measured for the water-like species at O^{br} .

Upon further hydrogen adsorption both the molecular

H_2 state at the Ru^{cus} site and the dissociated monohydride state at bridge-site surface oxygen atoms become populated. The formation of the hydroxyl groups is hereby found to intricately influence the reactivity at the neighboring cus sites, allowing for an increased back-donation further activating the H_2^{us} bond. This modification of the bonding properties at cus by hydrogen decoration at bridge is attributed to a bond order propagation mechanism, possibly special to this metallic oxide. It is argued that the resulting possibility of fine tuning the cus site reactivity by controlled modification of the bridge site population could be of relevance for catalytic applications, in particular partial oxidation reactions where a precise tuning of the bond strengths could be crucial to obtain high selectivities.

Acknowledgments

Q.S. is thankful for an Alexander von Humboldt fellowship. Valuable discussions with K. Jacobi, Y. Wang, J. Wang, C.Y. Fan, and G. Ertl are gratefully acknowledged.

Appendix

In order to ensure the needed numerical accuracy we particularly performed calculations with larger interstitial plane wave cutoffs and denser k-point meshes – the latter two being the most influential parameters in the FP-LAPW basis set. Some of these tests are sketched in this appendix. Specifically, we increased the cutoffs up to 36 Ry in several steps and doubled the k-point mesh to 36 k-points in the IBZ for (1×1) surface unit-cells. Table III lists the resulting bond lengths, bond angles, and binding energies for three characteristic phases involved in the present study: the bare $\text{RuO}_2(110)$ surface ($\text{O}^{\text{br}}/-$), a hydroxyl-group at bridge ($(\text{OH})^{\text{br}}/-$) and molecular hydrogen at cus ($\text{O}^{\text{br}}/\text{H}_2^{\text{cus}}$). It can be seen that the structural parameters of all three phases are well converged already at the lowest cutoff listed (20.25 Ry), let alone that the employed k-mesh has any influence. However, the absolute binding energies are not yet fully converged at this low cutoff, primarily due to the need to use very small muffin-tin spheres as discussed in the text. From the convergence behavior along the sequence 20.25 Ry \rightarrow 25 Ry \rightarrow 30.25 Ry \rightarrow 36 Ry we conclude

that only at a high cutoff of 30.25 Ry the latter quantities are converged to within 0.1 eV/H atom. Fortunately enough, relative energetic differences between similar geometries involving an equal number of O and H atoms converge much more rapidly. This is illustrated by a comparison of the binding energy of the hydroxyl group at bridge either in an upright or in the tilted configuration (listed in Table III): at all tested cutoffs between 20.25 Ry and 36 Ry this energetic difference is 0.1 eV/H atom, constant to within 0.01 eV/H atom. Correspond-

TABLE III: Computed bond lengths (d in Å), tilt angle (in °) and absolute binding energies (E_b in eV) as a function of interstitial plane wave cutoff and number of k-points for three phases characteristic for the present study.

$\text{O}^{\text{br}}/-$	$d_{\text{O}^{\text{br}}-\text{Ru}^{\text{br}}}$				$E_b(\text{O})$
20.25 Ry, 18 k	1.91				2.54
25 Ry, 18 k	1.90				2.46
25 Ry, 36 k	1.90				2.43
30.25 Ry, 18 k	1.91				2.43
36 Ry, 18 k	1.91				2.37

$(\text{OH})^{\text{br}}/-$	$d_{\text{O}^{\text{br}}-\text{Ru}^{\text{br}}}$	$d_{\text{H}^{\text{br}}-\text{O}^{\text{br}}}$	tilt	$E_b(\text{H})$
20.25 Ry, 18 k	2.06	0.97	40	0.71
25 Ry, 18 k	2.08	0.98	45	0.84
25 Ry, 36 k	2.08	0.98	46	0.82
30.25 Ry, 18 k	2.07	0.98	46	0.89
36 Ry, 18 k	2.07	0.97	46	0.91

$\text{O}^{\text{br}}/\text{H}_2^{\text{cus}}$	$d_{\text{O}^{\text{br}}-\text{Ru}^{\text{br}}}$	$d_{\text{H}-\text{Ru}^{\text{cus}}}$	$d_{\text{H}-\text{H}}$	$E_b(\text{H}_2)$
20.25 Ry, 18 k	1.92	1.89	0.81	0.38
25 Ry, 18 k	1.92	1.89	0.81	0.35
25 Ry, 36 k	1.92	1.89	0.81	0.34
30.25 Ry, 18 k	1.92	1.89	0.81	0.32
36 Ry, 18 k	1.92	1.89	0.81	0.30

ingly, we employed the manageable cutoff of 20.25 Ry for structural relaxations, vibrational calculations and when judging on the relative energetic sequence of similar structures. Only when absolute binding energies converged to within 0.1 eV/H atom are required, did we run additional calculations at 30 Ry, but with fixed geometry.

¹ V.E. Henrich and P.A. Cox, *The Surface Science of Metal Oxides* (Cambridge University Press, Cambridge, England, 1994).

² C. Noguera, *Physics and Chemistry at Oxide Surfaces* (Cambridge University Press, Cambridge, England, 1994).

³ D.P. Woodruff and T.A. Delchar, *Modern Techniques of Surface Science* (Cambridge University Press, Cambridge,

England, 1994).

⁴ P.I. Sorantin and K.H. Schwarz, *Inorg. Chem.* **31**, 567 (1992).

⁵ C.H.F. Peden and D.W. Goodman, *J. Phys. Chem.* **90**, 1360 (1986).

⁶ H. Over, Y.D. Kim, A.P. Seitsonen, S. Wendt, E. Lundgren, M. Schmid, P. Varga, A. Morgante, and G. Ertl,

- Science **282**, 1474 (2000).
- ⁷ H. Over and M. Muhler, Prog. Surf. Sci. **72**, 3 (2003).
 - ⁸ D.R. Rolison, P.L. Hagans, K.E. Swider, and J.W. Long, Langmuir **15**, 774 (1999).
 - ⁹ Y.D. Kim, A.P. Seitsonen and H. Over, Surf. Sci. **465**, 1 (2000).
 - ¹⁰ C.Y. Fan, J. Wang, K. Jacobi, and G. Ertl, J. Chem. Phys. **114**, 10058 (2001).
 - ¹¹ J. Wang, C.Y. Fan, K. Jacobi, and G. Ertl, Surf. Sci. **481**, 113 (2001); J. Chem. Phys. B **106**, 3422 (2002).
 - ¹² K. Reuter and M. Scheffler, Phys. Rev. B **65**, 035406 (2002).
 - ¹³ K. Reuter and M. Scheffler, Phys. Rev. B **68**, 045407 (2003).
 - ¹⁴ K. Reuter and M. Scheffler, Appl. Phys. A (*in press*).
 - ¹⁵ K. Reuter and M. Scheffler, Phys. Rev. Lett. **90**, 046103 (2003).
 - ¹⁶ Q. Sun, K. Reuter and M. Scheffler, Phys. Rev. B **67**, 205424 (2003).
 - ¹⁷ L. Zang and H. Kisch, Angew. Chem. Int. Ed. **39**, 3921 (2000).
 - ¹⁸ J. Wang, C.Y. Fan, Q. Sun, K. Reuter, K. Jacobi, M. Scheffler, and G. Ertl, Angew. Chem. Int. Ed. **42**, 2151 (2003).
 - ¹⁹ R.M. Dreizler and E.K.U. Gross, *Density Functional Theory* (Springer, Berlin, 1990).
 - ²⁰ P. Blaha, K. Schwarz and J. Luitz, WIEN97, *A Full Potential Linearized Augmented Plane Wave Package for Calculating Crystal Properties*, Karlheinz Schwarz (Techn. Universität Wien, Austria, 1999). ISBN 3-9501031-0-4.
 - ²¹ B. Kohler, S. Wilke, M. Scheffler, R. Kouba, and C. Ambrosch-Draxl, Comput. Phys. Commun. **94**, 31 (1996).
 - ²² M. Petersen, F. Wagner, L. Hufnagel, M. Scheffler, P. Blaha, and K. Schwarz, Comp. Phys. Commun. **126**, 294 (2000).
 - ²³ J.P. Perdew, K. Burke and M. Ernzerhof, Phys. Rev. Lett. **77**, 3865 (1996).
 - ²⁴ J.P. Perdew and Y. Wang, Phys. Rev. B **45**, 13244 (1992).
 - ²⁵ K.M. Glassford and J.R. Chelikowsky, Phys. Rev. B **47**, 1732 (1993).
 - ²⁶ C.E. Boman, Acta Chem. Scand. **24**, 116 (1970).
 - ²⁷ Y.S. Huang, H.L. Park and F.H. Ploock, Mater. Res. Bull. **17**, 241 (1982).
 - ²⁸ Lj. Atanasoska, W.E. O'grady, R.T. Atanasoski, and F.H. Pollak, Surf. Sci. **202**, 142 (1988).
 - ²⁹ V.E. Henrich and R.L. Kurtz, Phys. Rev. B **23**, 6280 (1981).
 - ³⁰ X.-G. Wang, A. Chaka and M. Scheffler, Phys. Rev. Lett. **84**, 3650 (2000).
 - ³¹ *CRC Handbook of Chemistry and Physics*, 81st ed. (CRC Press, Boca Raton FL, 2000).
 - ³² P.A. Thiel and T.E. Madey, Surf. Sci. Rep. **7**, 211 (1978).
 - ³³ D.D. Wagman *et al.*, *NBS Chemical Thermodynamic Data Base* (Nat. Bureau of Standards, Washington DC, 1965).
 - ³⁴ E. Clementi and S.J. Chakravorty, J. Chem. Phys. **93**, 2591 (1990).
 - ³⁵ B. Hammer and M. Scheffler, Phys. Rev. Lett. **74**, 3487 (1995).
 - ³⁶ F. Finocchi and J. Goniakowski, Phys. Rev. B **64**, 125426 (2001).
 - ³⁷ K. Reuter, D. Frenkel and M. Scheffler (*to be published*).
 - ³⁸ S. Wilke and M. Scheffler, Phys. Rev. B **53**, 4926 (1996).
 - ³⁹ M. Gruyters and K. Jacobi, Chem. Phys. Lett. **225**, 309 (1994).
 - ⁴⁰ M. Scheffler and C. Stampfl, *Theory of Adsorption on Metal Substrates*. In: Handbook of Surface Science, Vol. **2: Electronic Structure**, Eds. K. Horn and M. Scheffler (Elsevier, Amsterdam, 2000).
 - ⁴¹ K. Christmann, Surf. Sci. Rep. **9**, 1 (1988).
 - ⁴² A.S. Martensson, C. Nyberg and S. Andersson, Phys. Rev. Lett. **57**, 2045 (1986).
 - ⁴³ P.K. Schmidt, K. Christmann, G. Kresse, J. Hafner, M. Lischka, and A. Gross, Phys. Rev. Lett. **87**, 096103 (2001).
 - ⁴⁴ G.J. Kubas, R.R. Ryan, B.I. Swanson, P.J. Vergamini, and H.J. Wasserman., J. Am. Chem. Soc. **106**, 451 (1984).
 - ⁴⁵ R.H. Crabtree and D.G. Hamilton, J. Am. Chem. Soc. **108**, 3124 (1986).
 - ⁴⁶ G.J. Kubas, J. Less-Common Metals **172**, 475 (1991).
 - ⁴⁷ K.W. Zilm, R.A. Merrill, M.W. Kummer, and G.J. Kubas, J. Am. Chem. Soc. **108**, 7837 (1986).
 - ⁴⁸ L.S. van der Sluys, J. Eckert, O. Eisenstein, J.H. Hall, J.C. Huffman, S.A. Jackson, T.F. Koetzle, G.J. Kubas, P.J. Vergamini, and K.G. Caulon, J. Am. Chem. Soc. **112**, 4831 (1990).
 - ⁴⁹ H. Brunner, *Applied Homogeneous Catalysis with Organometallic Compounds* (VCH, Weinheim, 1996).
 - ⁵⁰ Y. Wang, J. Wang, C.Y. Fan, K. Jacobi, and G. Ertl (*private communication*).